Role of Surface Albedo For Explaining Differences of Modeled Greenland Ice Sheet Melt

by

Maxim Altan-Lu Shapovalov

A thesis accepted and approved in partial fulfillment of the

requirements for the degree of

Master of Science

in Geography

Thesis Committee:

Jonathan C. Ryan, Chair

Sarah W. Cooley, Member

University of Oregon

Spring 2024

THESIS ABSTRACT

Maxim Altan-Lu Shapovalov

Master of Science in Geography

Title: Role of Surface Albedo For Explaining Differences of Modeled Greenland Ice Sheet Melt

The Greenland Ice Sheet has been in a state of negative mass balance for the past several decades and is currently responsible for a substantial proportion of global sea-level rise. Accurate projections of ice sheet mass loss are therefore imperative, and a number of regional climate models (RCMs) have been developed for this purpose. However, a recent intercomparison (GrSMBMIP) of surface mass balance (SMB) models demonstrated substantial discrepancies between their individual projections. One likely explanation for model spread is inaccurate simulation of albedo, which determines the amount of shortwave radiation that is absorbed by the ice sheet surface. Here, we force a state-of-the-art surface energy balance model (IceModel v1.0) with four albedo products to investigate the sensitivity of meltwater production to different albedo parameterizations for the 2009-2022 period. The four albedo products include one product from satellite observations (MODIS MCD43A3), which we treat as "ground-truth", one atmospheric reanalysis (MERRA-2), and two RCMs (MAR v3.12.1 and RACMO2.3p2). We find that, for fifteen of automated weather stations located at the margins of the ice sheet, MAR and MERRA-2, on average, overestimate observed (MODIS) glacier ice albedo by +0.11 and +0.13, respectively, while RACMO underestimates it by -0.07. These biases mean that IceModel underestimates melt -36.3% and -27.1% when forced by albedo derived from MAR and MERRA-2, respectively. In contrast, IceModel overestimates melt by +5.5% when forced by albedo derived from RACMO. We also identify several compensating effects in our analysis. We also highlight the presence of counteractive errors of albedo representations in all models that result in diminished uncertainty. Specifically, RACMO tends to overestimate snow albedo, while generally underestimating glacier ice albedo, which results in an estimate that appears to be more accurate relative to observations. Ultimately, based on the partitioned information that we outline further in this thesis, we offer suggestions for future improvements in modeled albedo parameterizations.

ACKNOWLEDGMENTS

TABLE OF CONTENTS

LIST OF FIGURES

LIST OF TABLES

1. INTRODUCTION

Greenland Ice Sheet (GrIS) mass loss has been increasing since the 1990s and is now the single largest cryospheric contributor to observed global sea-level rise (Otosaka et al., 2023). The main mechanism by which the GrIS contributes to sea levels during the 21st century is via surface meltwater runoff (Enderlin et al., 2014; M. van den Broeke et al., 2009; M. R. van den Broeke et al., 2016), almost all of which is produced in the ablation zone (Steger et al., 2017). During the summer, when the downward shortwave radiation and near-surface air temperature reach annual maxima, the winter snowpack completely melts, exposing dark glacier ice (Ryan et al., 2019). Since glacier ice has low albedo, it produces more meltwater than snow, much of which is efficiently evacuated from the ice sheet into the ocean (Smith et al., 2017). Projections of global sea-level rise, in both the past and future, therefore depend on accurate knowledge of meltwater production in the GrIS ablation zone (M. van den Broeke et al., 2017).

Since there are few direct measurements of meltwater runoff, hindcasts and forecasts of meltwater production are traditionally provided by regional climate models (RCMs). These models couple high-resolution atmospheric dynamics with multilayer snow models that simulate mass and energy exchange at the ice sheet surface (e.g. Fettweis et al., 2013). There are several RCMs that have been developed for this purpose, all of which have slightly different model physics, parameterizations, and numerical methods.

Uncertainties in modeled meltwater runoff are usually assessed using intercomparison projects. The primary goal of an intercomparison project is to run a set of numerical climate models under standardized boundary conditions and compare their results. The ensemble mean is then often used as a "best estimate" in studies of the GrIS's total mass balance (e.g. Shepherd et al., 2020). A number of intercomparison projects have been carried out to investigate GrIS Surface Mass Balance (SMB; e.g., Fettweis et al., 2020; Rae et al., 2012; Vernon et al., 2013). The most recent project, named the "Greenland Ice Sheet Surface Mass Balance Model Intercomparison Project" (GrSMBMIP), compared SMB estimates of thirteen climate models constrained to a common time period, ice-sheet mask, spatial grid, and boundary forcing data (Fettweis et al., 2020). The application of these constraints allowed for more realistic inter-comparability in modeled SMB estimates and refined uncertainty.

In general, model intercomparison exercises are useful for identifying how well models agree in their spatial and temporal patterns. However, despite parametrical constraints, intercomparison studies are unable to attribute differences in modeled meltwater production to specific processes. If all models over- or under-estimate one of these processes (e.g. absorption of shortwave radiation), for example, this may be an issue since the ensemble mean will be biased by an unknown amount. An alternative approach for identifying processes responsible for differences in meltwater production can be achieved using sensitivity analysis. This approach involves systematically varying one or more input parameters while keeping all the others the same. The isolated variation of select variables allows for more direct attribution of model output to particular processes. Thus, for detecting and/or attributing biases in modeled meltwater production to specific processes, the sensitivity analysis approach may be more suitable than intercomparison.

In this study, we aim to investigate the role of albedo in controlling discrepancies in melt as modeled by RCMs. We focus on albedo because it plays a crucial role in controlling the absorption of incoming shortwave radiation and is a key determinant of ablation for the GrIS (Braithwaite & Olesen, 1990; Brock et al., 2000; Knap & Oerlemans, 1996; M. R. van den Broeke et al., 2011). Assessing the effect of different models' albedo on meltwater estimates is therefore critical for evaluating the suitability of RCM albedo parameterizations. To do this, we employ a surface energy balance model, IceModel, which allows for meteorological forcings and is designed to capture complex subsurface melt/refreezing processes in the glacier column. We force this model using data from fifteen automated weather stations (AWSs) positioned on the margins of the GrIS. The four sources of albedo that we compare are derived from Moderate Resolution Imaging Spectroradiometer (MODIS) satellite observations, one atmospheric reanalysis (MERRA-2), and two RCMs (MARv3.12.1 and RACMO2.3p2), all of which are described in detail in Section 2. Since we treat MODIS albedo as ground-truth, we refer to this source of albedo as "observations" from now onwards. To conduct our study, we first compare average summer (JJA) albedo of each model for every AWS. We then simulate melt using these different albedo values to demonstrate the extent to which albedo is responsible for melt differences at the AWS sites. The findings from this study provide uncertainty bounds in modeled albedo and melt, as well as directions for future development of albedo parameterizations of models compared in this study.

2. METHODS

2.1. IceModel

The primary tool used in this study is IceModel (v1.0), a physically-based surface energy balance (SEB) model that computes meltwater production and refreezing by solving the one-dimensional mass, thermal, and spectral radiative heat transfer equation (M. Cooper et al., 2021; Liston et al., 1999):

$$\frac{\partial H_i}{\partial t} = \frac{\partial}{\partial z}\left[(k_i + k_v)\frac{\partial T_i}{\partial z}\right] - \frac{\partial q}{\partial z} \tag{1}$$

where H_i is enthalpy (W m^{-3}), t is time, T_i (K) is ice temperature, z (m) is the vertical coordinate, k_i (W m^{-1} K^{-1}) is glacier ice thermal conductivity, k_v is the water vapor diffusion coefficient, and $\partial q/\partial z$ (W m^{-3}) is the net solar radiative heat flux. IceModel replicates an ice column featuring dynamic changes in ice, air, water vapor, and liquid water content over time. An important feature of IceModel is its ability to allow sunlight to penetrate the glacier ice, facilitating subsurface melting rather than concentrating all available energy on an extremely thin surface layer. IceModel's development was informed by measurements of physical ice surface properties collected during field campaigns on the GrIS ablation zone, and evaluated by comparison with direct measurements of meltwater runoff from glacier ice (M. G. Cooper et al., 2021; Pitcher & Smith, 2019; Rennermalm et al., 2013; Smith et al., 2015, 2017; Yang et al., 2018). In order to account for most of the melt, a period of April 1 to October 1 was chosen for analysis in each simulation year.

2.2. Meteorological forcing

With the exception of albedo, the physical input parameters (Table 1) used to force IceModel are derived from AWSs maintained by the Greenland and Denmark Geological Survey's (GEUS) Programme for Monitoring the Greenland Ice Sheet (PROMICE) (Tables 1 & 2; Fausto et al., 2021). Initially, the study focused on three AWSs in the western GrIS, also known as the K-transect: KAN-L, KAN-M, and KAN-U, where L stands for lower (670 m), M for middle (1270 m), and U for upper (1840 m; Fig. 1). The choice of the K-transect was mainly due to the fact that there are recorded meteorological data on areas of the ice sheet that fully (KAN-L), partially (KAN-M), and do not (KAN-U) expose glacier ice. This coverage is

11

preferable because it provides unique insight on how meteorological variables and processes change with different levels of glacier ice exposure.

Table 1. Physical parameters from AWSs used for IceModel forcing.

Physical Measurement	PROMICE Name	Units in IceModel
Air Temperature	t_u	K
Downwelling Shortwave Radiation	dsr	W m-2
Downwelling Longwave Radiation	dlr	W m-2
Albedo	albedo	–
Sensible Heat Flux	dshf_u	W m-2
Latent Heat Flux	dlhf_u	W m-2
Cloud Fraction	cc	%
Surface Temperature	t_surf	K
Air Pressure	p_u	Pa
Wind Speed	wspd_u	m s-1
Wind Direction	wdir_u	°
Relative Humidity	rh_u	%

Table 2. Metadata for the PROMICE automatic weather station network. Latitude, longitude, and elevation (in meters above sea level) are extracted from (Fausto et al., 2021). The last column indicates whether glacier ice is exposed for at least 1 hour at a given station. We compute this based on average 2009-2022 MODIS albedo at a given weather station; "yes" for albedo value of ≤0.55, "no" for >0.55.

AWS	Latitude	Longitude	Elevation (m.a.s.l)	Exposes glacier ice
KAN-L	67.0955	49.9513	670	yes
KAN-M	67.067	48.8355	1270	yes
KAN-U	67.0003	47.0253	1840	no
KPC-L	79.9108	24.0828	370	yes
KPC-U	79.8347	25.1662	870	no
NUK-L	64.4822	49.5358	530	yes
NUK-U	64.5108	49.2692	1120	yes
QAS-L	61.0308	46.8493	280	yes
QAS-U	61.1753	46.8195	900	yes
SCO-L	72.223	26.8182	460	yes
SCO-U	72.3933	27.2333	970	yes

THU-L	76.3998	68.2665	570	yes
THU-U	76.4197	68.1463	760	no
UPE-L	72.8932	54.2955	220	yes
UPE-U	72.8878	53.5783	940	yes
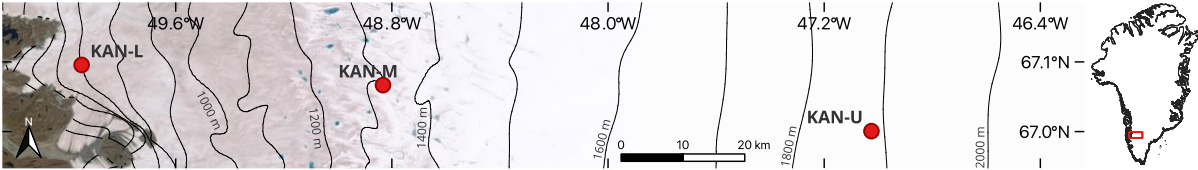
Figure 1. Close-up view of automated weather stations in the K-transect in Southwest Greenland. L stands for lower, M for middle, and U for upper. KAN-L is positioned in the visibly darker ablation zone with exposed glacier ice. KAN-U is in the accumulation zone where no glacier ice is exposed.

The analysis was then further expanded across six other AWS pairs along the ice sheet margins in order to identify whether our findings at the K-transect extended to other regions of the GrIS (Fig. 2). The study period was defined as 2009 to 2022, constrained by earliest available data from the AWSs and the latest accessible data from the different models. Since there were data gaps in some of the AWS records, we discarded several years from the analysis (Fig. 3).
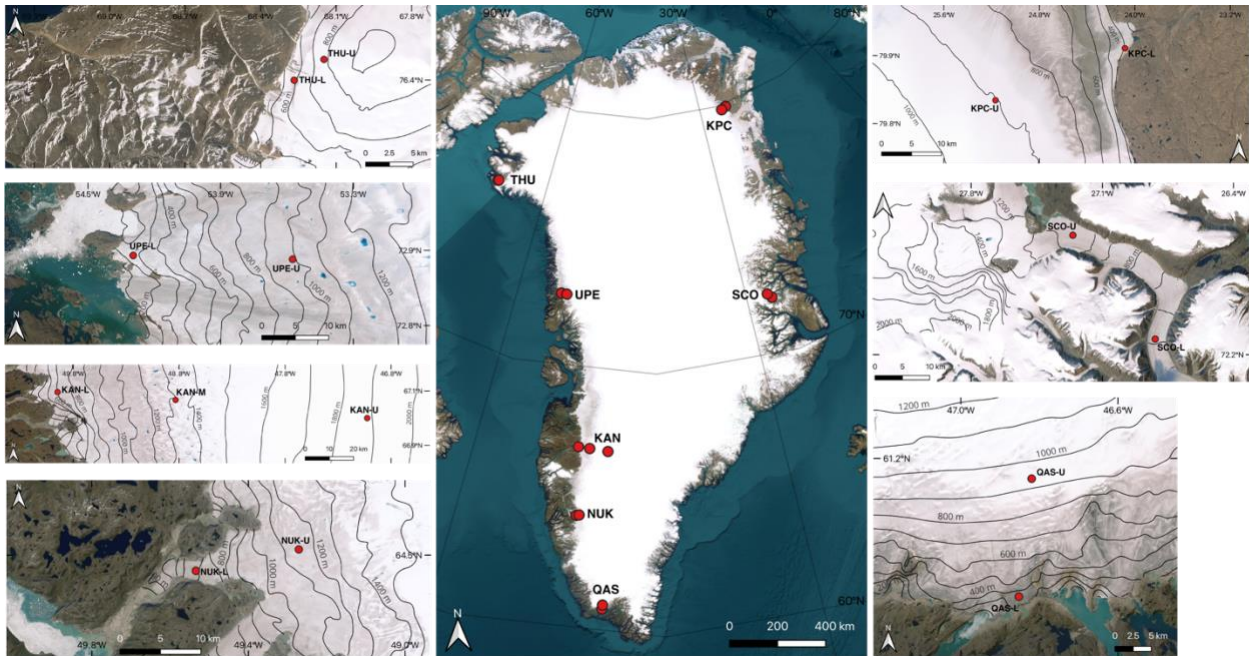
Figure 2. Locations of the 15 PROMICE automated weather stations used in this study on the Greenland Ice Sheet (central panel). Each side panel shows the detailed map of each AWS

13

pair/array. In each pair/array, the lower stations (-L) are lower in elevation and are closer to the margins of the ice sheet.

	KAN-L	KAN-M	KAN-U	KPC-L	KPC-U	NUK-L	NUK-U	QAS-L	QAS-U	SCO-L	SCO-U	THU-L	THU-U	UPE-L	UPE-U
2009	blue	blue	grey	grey	grey	blue	grey	grey	blue	grey	blue	grey	grey	blue	blue
2010	blue	blue	blue	grey	blue	grey	grey	grey	blue	blue	grey	blue	blue	blue	blue
2011	blue	blue	blue	grey	blue	grey	grey	blue	grey	blue	blue	grey	grey	grey	blue
2012	blue	blue	blue	blue	grey	grey	grey	blue	blue	blue	blue	grey	blue	blue	blue
2013	blue	blue	blue	blue	blue	grey	grey	blue	grey	blue	blue	blue	blue	grey	blue
2014	blue	grey	blue	blue	blue	grey	grey	blue	blue	blue	blue	blue	blue	blue	blue
2015	blue	blue	blue	blue	blue	grey	blue	blue	grey	blue	blue	blue	grey	blue	blue
2016	blue	blue	blue	blue	blue	blue	blue	blue	grey	blue	blue	blue	blue	blue	blue
2017	blue	blue	blue	blue	blue	blue	blue	blue	grey	blue	blue	blue	blue	blue	blue
2018	blue	blue	blue	grey	blue	blue	blue	blue	blue	blue	blue	grey	blue	blue	blue
2019	blue	blue	blue	blue	blue	blue	grey	blue	blue	blue	blue	blue	grey	blue	blue
2020	blue	blue	blue	blue	blue	blue	grey	grey	grey	blue	blue	grey	blue	blue	blue
2021	blue	blue	blue	blue	blue	grey	blue	grey	grey	blue	blue	grey	blue	blue	blue
2022	blue	blue	blue	blue	blue	grey	grey	grey	blue	blue	blue	blue	grey	blue	blue
Total	14	13	13	10	12	6	5	9	7	13	13	8	9	12	14

Figure 3. Data years that were (blue) and were not (grey) used for each AWS.

2.3. Albedo Datasets

We forced IceModel with albedo from two regional climate models (RCMs) and one atmospheric reanalysis product (Table 3; Fig. 4). To evaluate the accuracy of modeled albedo, and its impact of melt, we also forced IceModel with albedo data derived from MCD43A3 which we considered to be ground-truth. A full description of these albedo data is provided in the next sections.

Table 3. Details of surface albedo data sources used in the study.

Name	Version/product	Spatial Resolution	Native Temporal Resolution	Climate Forcing	Reference
MODIS	MCD43A3.061	500 m	1 day	Observed	(C. Schaaf & Wang, 2021)
MERRA-2	M2T3NXGLC_5.12.4	0.5°x0.625°	3 hours	MERRA-2	(Global Modeling and Assimilation Office (GMAO), 2015)
MAR	3.12.1	10 km	1 day	ERA5	(Tedesco & Fettweis, 2020)
RACMO	2.3p2	5.5 km	1 day	ERA5	(Noël et al., 2019)
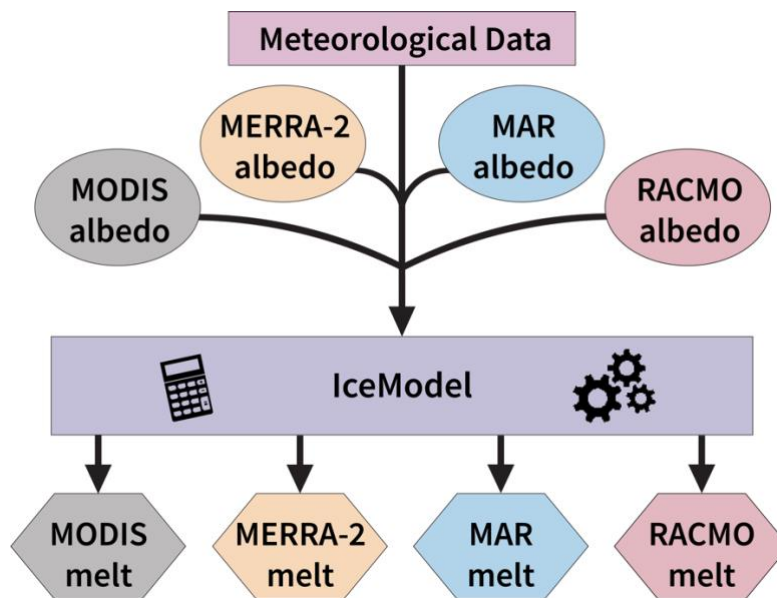
Figure 4. Flowchart showing the workflow behind IceModel simulations.

We note here that although albedo data is provided by the AWS, there were substantial gaps in these measurements that were too large to effectively patch for use in IceModel simulations. We discovered that even the most complete summer albedo AWS dataset had on average 51% missing values, which prompted us to establish a threshold for determining whether a dataset was complete enough to be forced into IceModel. The average gap size was 12 hours, which is most likely due to the fact that hourly albedo is not calculated when the sun hits the top of the radiometer at angles less than 20° (Fausto et al., 2021). We used linear interpolation to fill the gaps of missing data. Through visual inspection, we decided that a dataset should be discarded if its data was >65% incomplete because past that point, no patching method was able to fill the gaps in a way that would reflect the diurnal albedo variations. Ultimately, a significant portion (17%) of in-situ summer albedo data was too unreliable to use, which prompted us to turn to other datasets that would serve as comparable substitutes. Aside from incomplete summer albedo data, another reason why we decide to use a different albedo dataset for comparison with other models is the AWS's poor spatial representation of the ice sheet surface at large. The ground footprints of AWS-mounted pyranometers fail to capture the full spatial heterogeneity of the ice surface, resulting in overestimations in surface albedo during the melt season (Ryan, Hubbard, Irvine-Fynn, et al., 2017).

2.3.1. MODIS

We forced IceModel with albedo data from the MCD43A3 (version 6.1) black-sky albedo for shortwave broadband product. MCD43A3 has a spatial resolution of 500 m and is produced using atmospherically corrected MODIS reflectance data collected over 16 days, centered on the specific day. A semi-empirical bidirectional reflectance distribution function (BRDF) model is employed to calculate bi-hemispherical reflectance based on these reflectance measurements (C. B. Schaaf et al., 2002). We chose to use shortwave (0.3-5.0 µm) broadband albedo to match the wavelength interval of MAR (0.3-2.8 µm) that is outlined in the detailed descriptions of MAR's albedo scheme by Brun et al. (1992) and Lefebre et al. (2003). We also opted to utilize black-sky albedo instead of white-sky albedo because (Stroeve et al., 2005) demonstrated that the two are virtually identical for typical solar noon zenith angles over Greenland. We considered this simulation our "ground-truth" due to concerns about the quality of albedo measured by the AWSs mentioned earlier. The accuracy of MODIS albedo is known to be less reliable during non-melting periods pre-April and post-September, which are characterized by increased solar zenith angles (Box et al., 2012). We thus chose to focus on albedo and its effects on melt for the months of June, July, and August, which also coincides with the time when surface albedo has the largest impact on SMB.

Despite being based on satellite observations, MCD43A3 contains unrealistic albedo values due to undetected clouds and low solar angles. We filtered these values by setting thresholds consistent with previous studies. The highest albedo was capped at 0.84 based on in situ observations of Konzelmann & Ohmura (1995), which imply that albedo values above that are unrealistic for snow under clear-sky conditions. For the lower limit of the darkest possible glacier ice albedo, a value of 0.30 was chosen based on a conservative mean of lowermost albedos noted in Van As et al. (2013), Antwerpen et al. (2022), and Wehrlé et al. (2021). After filtering, we resampled this product to a 1-hour interval via linear interpolation to match the temporal resolution of the other meteorological variables used to force IceModel.

2.3.2. MERRA-2

The Modern-Era Retrospective analysis for Research and Applications, Version 2 (MERRA-2) is NASA's global atmospheric reanalysis product that provides climate data with high temporal resolution on a global scale (Global Modeling and Assimilation Office (GMAO),

2015). The specific product used in this study is M2T3NXGLC's (version 5.12.4) aggregated snow ice broadband albedo (SNICEALB). To simulate surface conditions, MERRA-2 implements the Goddard Earth Observing System model, version 5 (GEOS-5; Molod et al., 2015) integrated with a modified snow hydrology model by Stieglitz et al. (2001) to parameterize glacial thermodynamic processes. Surface albedo is calculated as a linear function of snow density in the uppermost layer based on surface radiative properties described by Greuell & Konzelmann (1994). Although MERRA-2 has a 15-layer ice column that allows for conduction of heat below the snow-ice interface, there is no parameterization for glacier ice albedo which is fixed at a value of 0.60 (Cullather et al., 2014).

2.3.3. MAR

The Modèle Atmosphérique Régional, version 3.12.1 (MAR) is a coupled land-atmosphere RCM that incorporates the CROCUS snow hydrology model (Brun et al., 1992) to simulate fluxes in the snowpack and simulate snow grain properties and their effect on surface albedo (Alexander et al., 2014; Fettweis, 2007). MAR calculates albedo based on cloudiness and zenithal angle, as well as the size and shape of snow grains based on CROCUS snow albedo parameterizations (Brun et al., 1992; Fettweis et al., 2011; Lefebre et al., 2003). Glacier ice albedo is quasi constant as it varies between 0.50 and 0.55; however, in the MARv3.12.1 provided by the model author, the glacier ice albedo does not lower than 0.55. The justification for using constant ice albedo is that it provides better results relative to previous parameterizations, which suggest that are too low in some parts of the GrIS (personal communication with the model author, Xavier Fettweis). The version of MAR used in this study was forced by ERA5 reanalysis (Hersbach et al., 2020).

2.3.4. RACMO

The polar version of Regional Atmospheric Model version 2.3p2 (RACMO) is an RCM that contains a multilayer snow module simulating meltwater percolation, retention and refreezing in firn (Ettema et al., 2010). Snow albedo is calculated based on snow grain size, solar zenith angle, cloud cover, and impurity concentration in the snow (van Angelen et al., 2012). Glacier ice albedo is prescribed from a MODIS albedo product (MCD43A3, 500-m, 16-day) as the lowest 5% of the surface albedo values averaged over the 2000-2015 period. The motivation behind applying the selective 5% method is its increased resilience to outliers compared to the

absolute minimum background albedo, aligning more closely with the multi-year minimum albedo (van Angelen et al., 2012). Minimum/maximum ranges are applied so that glacier ice albedo cannot be lower than 0.3 or higher than 0.55 (Fettweis et al., 2020; Noël et al., 2019; van Angelen et al., 2012). Similar to MAR, the version of RACMO used in this study was forced by ERA5 reanalysis (Hersbach et al., 2020).

2.4.   Albedo Categorization

In order to better understand the differences in simulated modeled, we categorized albedo from each model into five periods. Periods P1 and P5 represent times of the year when both MODIS and model are characterized by snow albedo (i.e. >0.60 for MERRA-2 and >0.55 for MAR and RACMO). P3 is when both the model and MODIS are characterized by glacier ice. P2 and P4 are periods when observations and models disagree about surface type (i.e. snow vs. glacier ice). Categorizing our data as described enables insight into the processes responsible for albedo differences (i.e. snow albedo in P1 and P5, glacier ice albedo in P3, and timing of glacier ice exposure in P2 and P4).

3. RESULTS

We note here some terminology that we use to improve the readability of the Results and Discussion sections. We refer to MARv3.12.1 simply as "MAR" and RACMO2.3p2 as "RACMO". The term "observed albedo" represents MODIS albedo (MCD43A3 product) and the term "observed melt" represents melt from IceModel when forced with MODIS albedo. It is important to note here that the term "MERRA-2 melt" represents melt simulated by IceModel when forced with MERRA-2 albedo, not melt from MERRA-2. Likewise, "MAR melt" and "RACMO melt" represents melt simulated by IceModel when forced with MAR and RACMO albedo, respectively. Consequently, differences in melt between different models can be solely attributed to differences in simulated albedo. We first describe our findings for weather stations on the K-transect. We then extend our analysis to six pairs of weather stations located in other regions of the ice sheet. We define "summer" as June, July, and August. All values represent the climatological median for the 2009-2022 study period. The spread around the median (i.e. "±") is represented by the interquartile range unless stated otherwise.

3.1. The K-transect

Observed albedo from MODIS exhibits seasonal variation at all K-transect sites over the 2009-2022 study period (Fig. 5a). Albedo at KAN-L steadily declines from May (0.71 ± 0.04; median ± IQR), reaches an absolute minimum at the end of July (0.41 ± 0.02), and begins to increase to a value of 0.73 ± 0.06 by mid-September. At KAN-M, high albedo persists throughout April with an average of 0.81 ± 0.01, then generally decreases until the first week of August to 0.46 ± 0.08, and steadily increases starting mid-August to 0.79 ± 0.01 by the end of September. At KAN-U, high surface albedo (0.83 ± 0.01) persists throughout April and May, decreases to 0.72 ± 0.03 in the second half of July, and the steadily increases to a relatively stable 0.83 ± 0.003 in the second week of September.

As expected, IceModel simulates more melt at KAN-L, where observed albedo is lowest, and less melt at KAN-U, where observed albedo is highest (Fig. 5b). KAN-L has the lowest average summer albedo (0.45 ± 0.04) of the three AWS sites and yields 2.84 ± 0.36 m of melt by the end of summer. As elevation rises, air temperatures become colder, and the exposure of glacier ice is delayed. The average summer albedo at KAN-M is 0.57 ± 0.08, producing 0.82 ±

19

0.52 m of melt. Lastly, at KAN-U, glacier ice is never exposed, the average albedo is 0.77 ±

0.03, and only a negligible amount (0.008 ± 0.009 m) of meltwater is produced during the

summer.
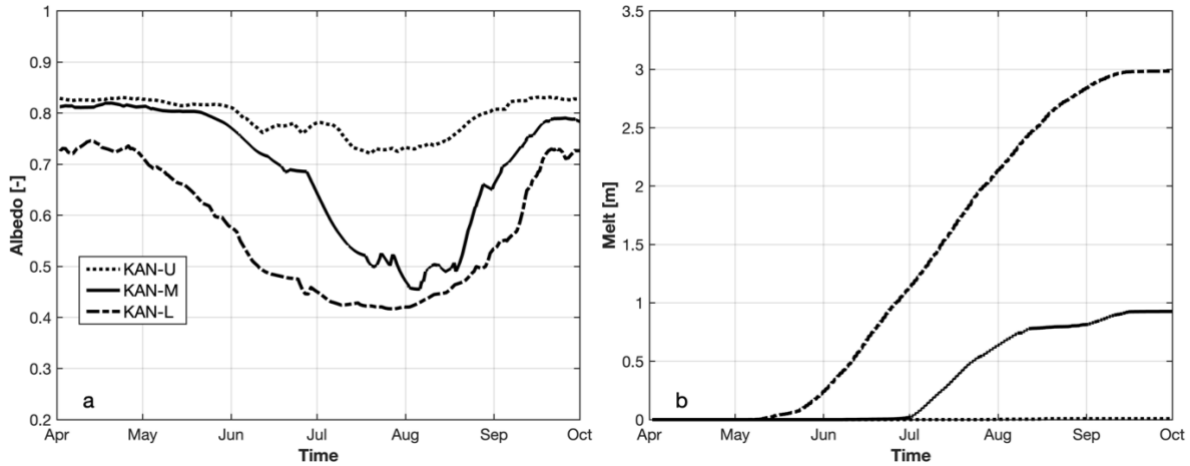
Figure 5. a) MODIS albedo. Albedo lower than 0.55 indicates conditions in which snow has melted and glacier ice is exposed. b) Melt derived from IceModel with MODIS-albedo of each AWS in the K-transect. Melt production is highest in July and August, and lowest in the colder seasons. The minimal melt at KAN-U relative to other stations pertains because it has the highest elevation.

Albedo simulated by MERRA-2 exhibits the least elevational variability across the K-

transect (Fig. 6). Summer albedo averages are 0.58 ± 0.01, 0.61 ± 0.03, and 0.71 ± 0.06 at KAN-

L, KAN-M, and KAN-U, respectively. The range in summer albedo, from the lower to the upper

site, therefore, differs by only 0.13 ± 0.05 during the study period. Relative to observed albedo,

MERRA-2 overestimates average summer albedo at KAN-L by +0.13 (Fig. 6a). As a result, melt

is underestimated by -0.95 m (-34%) (Fig. 7a). MERRA-2 only slightly overestimates average

summer albedo at KAN-M by +0.04 (Fig. 6b), leading to similar melt relative to observed (+0.08

m or +9.8%) (Fig. 7b). At KAN-U, however, MERRA-2 underestimates albedo by -0.06 (Fig.

6c), leading to an overestimation of modeled melt by +0.30 m (Fig. 7c). We choose to not

display the percentage differences of melt for the upper site (KAN-U) because, relative to KAN-

M and KAN-L, the produced values are very small, and thus can vary dramatically in terms of

percentages. This can be very misleading and attract more attention to itself when it is in fact less

significant than the lower-elevation stations.

Albedo simulated by RACMO, on the other hand, displays the most elevational variability across the K-transect. The summer albedo averages 0.30 ± 0.02 at KAN-L, 0.64 ± 0.12 at KAN-M, and 0.82 ± 0.04 at KAN-U, displaying a spread of 0.52 ± 0.18 from the lowermost to the uppermost site (Fig. 6). Relative to observed albedo, RACMO underestimates albedo by -0.15 at KAN-L, and overestimates by +0.07 and +0.05 at KAN-M and KAN-U, respectively. Translating this to melt, RACMO overestimates melt by +0.33 m (+12%) at KAN-L, and underestimates melt by -0.07 m (-8.5%) and -0.0075 m at KAN-M and KAN-U, respectively (Fig. 7).

Summer albedo simulated by MAR averages 0.55 ± 0.004 at KAN-L, 0.65 ± 0.07 at KAN-M, and 0.77 ± 0.04 at KAN-U (Fig. 6). Relative to observations, MAR overestimates albedo by +0.10 and +0.08 at KAN-L and KAN-M, respectively, which results in underestimated melts by -0.57 m (-20%) and -0.25 m (-30%), respectively. At KAN-U, MAR overestimates average summer albedo by +0.0012, leading to overestimated melt by +0.026 m.
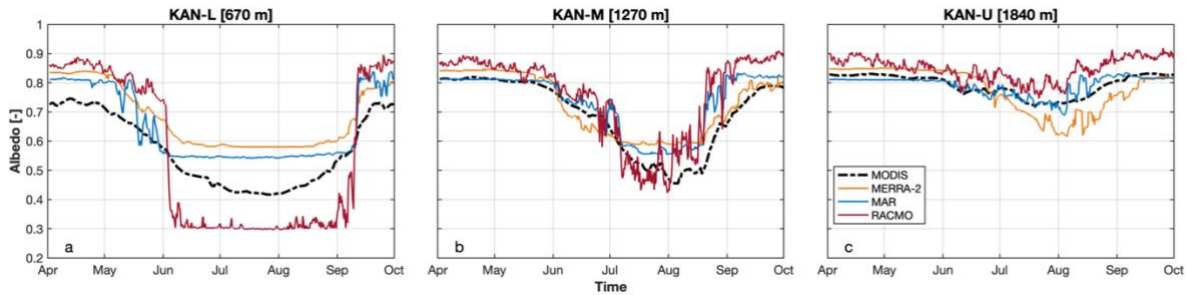
Figure 6. Average albedos of all models in the study at a) KAN-L, b) KAN-M, and c) KAN-U.
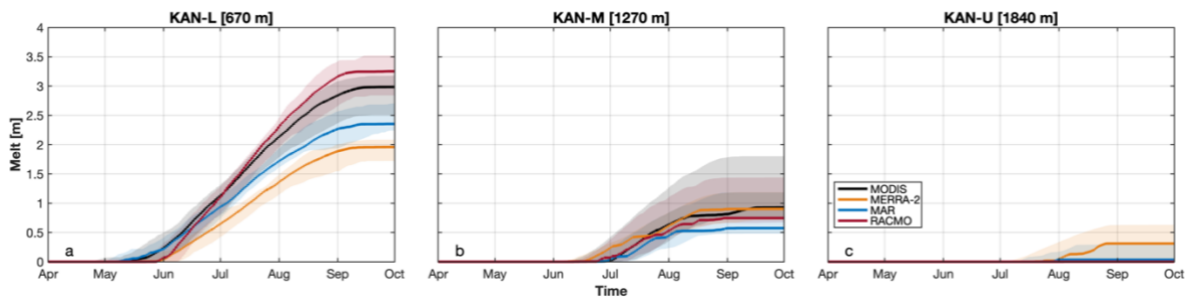
Figure 7. Average produced meltwater with albedo forcings from all the models in the study at a) KAN-L, b) KAN-M, and c) KAN-U. Solid line represents the 50th quantile (median) and the shaded area is the spread from the 25th to the 75th quantiles.

Generally, models simulate snow albedo more accurately than glacier ice (Fig. 8). During periods of snow cover (P1 and P5), MERRA-2 albedo values deviate from observations by only ±0.012, although MAR has a slight negative bias of -0.029, and RACMO has a slight positive bias of +0.052. This translates directly to small differences in modeled melt during P1, where all models have more conservative estimates relative to observations (-0.020 m for MERRA-2, -0.023 m for MAR, and -0.089 m for RACMO; Fig. 9).

Differences between modeled and observed albedo are larger for glacier ice (Fig. 8). When glacier ice is exposed (P3), both MERRA-2 and MAR overestimate albedo by +0.11 (+24.4%) and +0.10 (+23.6%), respectively. RACMO, on the other hand, underestimates albedo by -0.07 (-14.7%). MERRA-2 and MAR therefore underestimate melt during this period (-0.37 m [-27.5%] and -0.53 m [-38.8%], respectively), while RACMO, on the other hand overestimates by +0.21 m (+15.8%; Fig. 9).
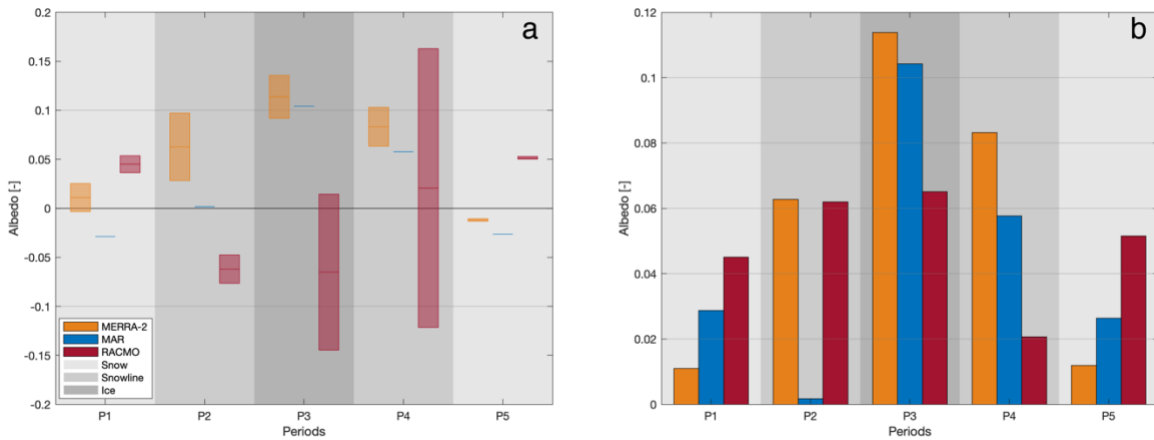
Figure 8. a) Bias and b) RMSE of model albedo relative to MODIS at the K-transect.
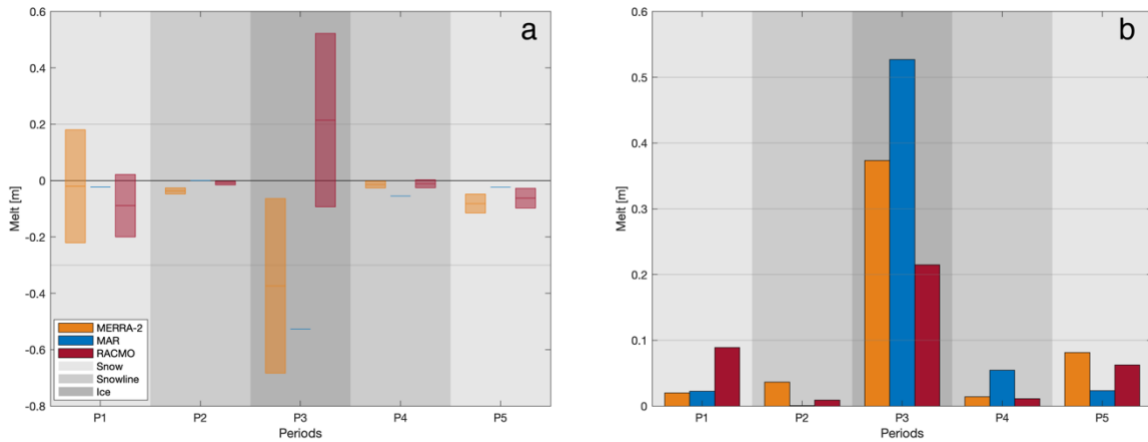
Figure 9. a) Bias and b) RMSE of melts derived with individual model albedos relative to MODIS at the K-transect.

Along the K-transect, MAR captures the timing of glacier ice exposure extremely accurately relative to observations during the snow to glacier ice transition period (P2), with a average delay of only 0.25 days during our study period (Fig 9, 10). RACMO tends to expose glacier ice 2.2 days before observations and therefore underestimates albedo by -0.062 during this period. MERRA-2, on the other hand, tends to expose glacier ice later by 5.6 days relative to observations and therefore overestimates albedo by +0.063. The positive biases in albedo values during the transition period from glacier ice to snow (P4) for all models are indicative of them shifting to snow earlier than MODIS. MAR is the first to transition to snow, 17.4 days before observations, with MERRA-2 being second (3.5 days), and RACMO the closest to MODIS with only a 0.5-day premature covering of glacier ice (Fig. 10).

By combining the number of days in P2 and P4, we find that all models underestimate the average total glacier ice exposure relative to observations: MAR by 17.7 days, MERRA-2 by 9.1 days, and RACMO by 1.3 days. MAR, which exposes glacier ice for the shortest period of time relative to observations, underestimates cumulative melt by -0.63 m (-32.0%), with MERRA-2 following closely behind with an underestimate of -0.53 m (-26.9%). In RACMO's case, the average yearly melt is underestimated by only -0.04 m (-2.2%), which is significantly lower than the melt overestimate produced during P3 (+0.21 m [+15.8%]), when both products expose glacier ice. This is due to RACMO's underestimation of melt during every other period, which causes to counteract the summer overestimation. In other words, when ice is not exposed,

RACMO overestimates albedo (Fig. 8a) and thus produces less melt than observations (Fig. 9a). However, when glacier ice *is* exposed, RACMO underestimates albedo and, as a result, simulates more generated meltwater relative to observations.
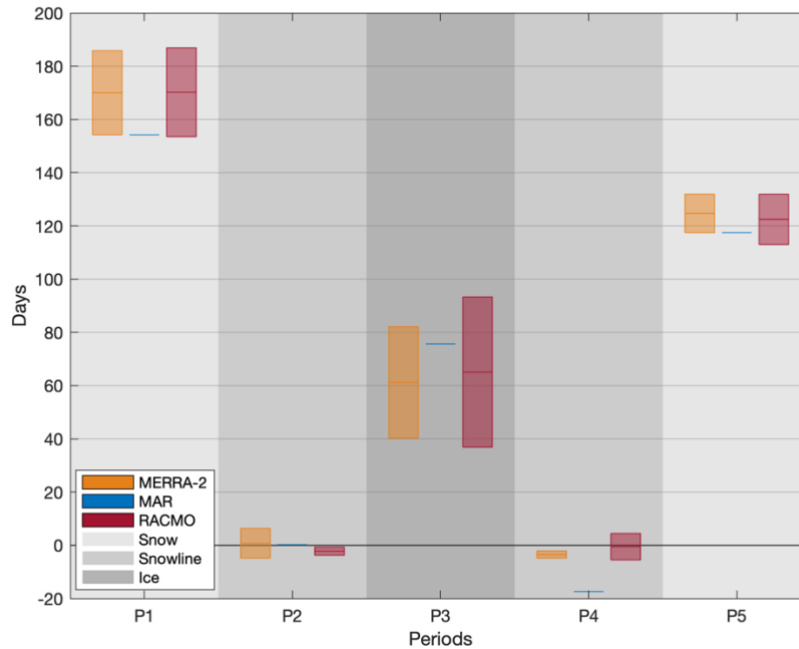
Figure 10. Average duration of each period for each non-observation model at the K-transect. When comparing one of the three models to MODIS, Snow is a time period when both indicate snow albedo, Snowline is when one is snow albedo while the other exposed glacier ice (0.6 for MERRA-2, 0.55 for the rest), and Ice is when both exposed glacier ice. For P2/P4, positive values indicate a delay in glacier ice exposure/covering.

3.2.   All Weather Stations

Across all 15 AWS, MAR generally underestimates snow albedo (-0.026 [-3.1%]; Fig. 11a, P1 and P5), overestimates glacier ice albedo (+0.11 [25.8%]; Fig. 11a, P3), underestimates average yearly melt (-0.60 m [-36.3%]; Fig. 12a), and exposes glacier ice 30 days less (Fig. 13) relative to observations. MERRA-2 follows almost identical trends found with MAR: overestimates glacier ice albedo (+0.13 [27.5%]), underestimates yearly melt (-0.45 m [27.1%]), and underexposes glacier (-18.7 days). The only difference is with representation of snow: in the first half of the year (P1), MERRA-2 slightly overestimates albedo (+0.0024 [0.3%]), while, similar to MAR, underestimates it by -0.011 (-1.3%) in the post-summer accumulation season (P5). Lastly, RACMO tends to overestimate snow albedo (+0.052 [+6.2%]), underestimate

glacier ice albedo (-0.067 [-15.7%]), overestimate cumulative melt (+0.091 m [5.5%]), and underexposes glacier ice (-3.2 days) relative to observations.

Figure 11. a) Bias and b) RMSE of model albedo relative to MODIS across all AWS.

Figure 12. a) Bias and b) RMSE of melts derived with individual model albedos relative to MODIS across all AWS.
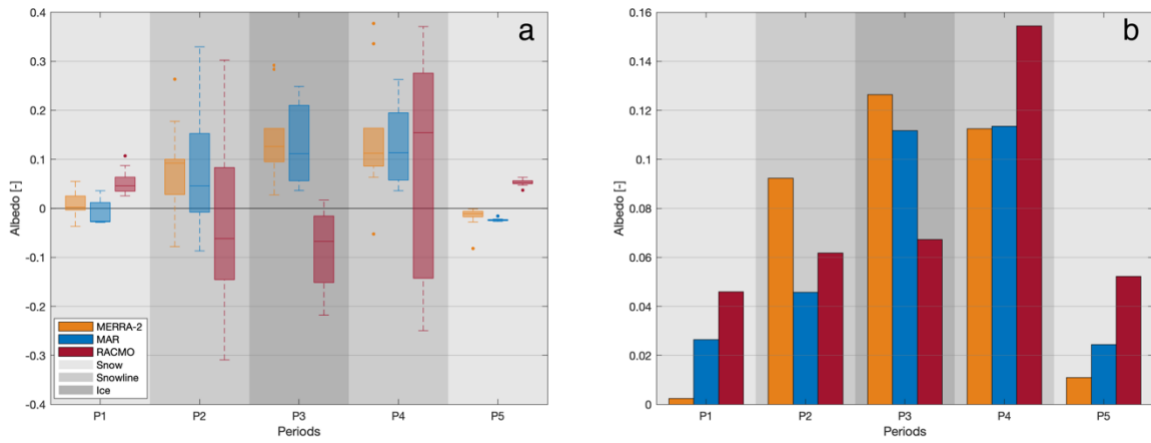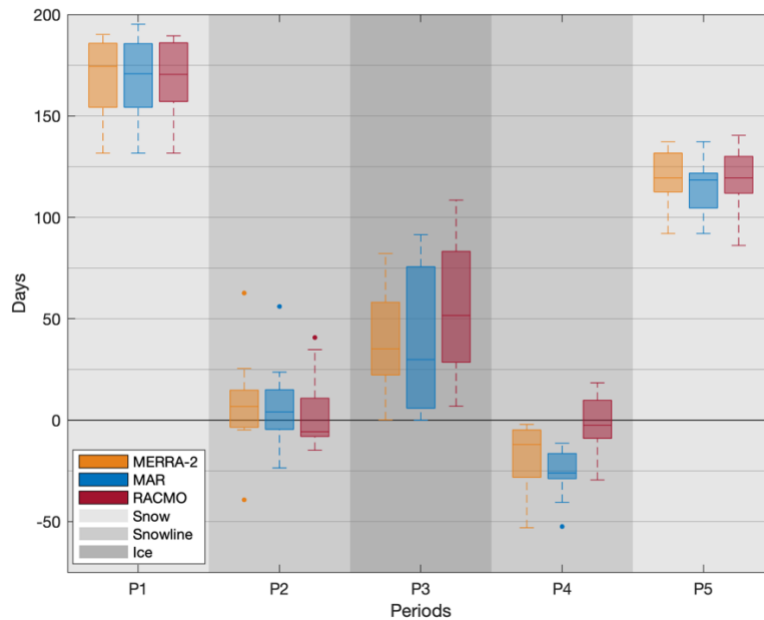
Figure 13. Average duration of each period for each non-observation model at the K-transect. When comparing one of the three models to MODIS, Snow is a time period when both indicate snow albedo, Snowline is when one is snow albedo while the other exposed glacier ice (0.6 for MERRA-2, 0.55 for the rest), and Ice is when both exposed glacier ice. For P2/P4, positive values indicate a delay in glacier ice exposure/covering.
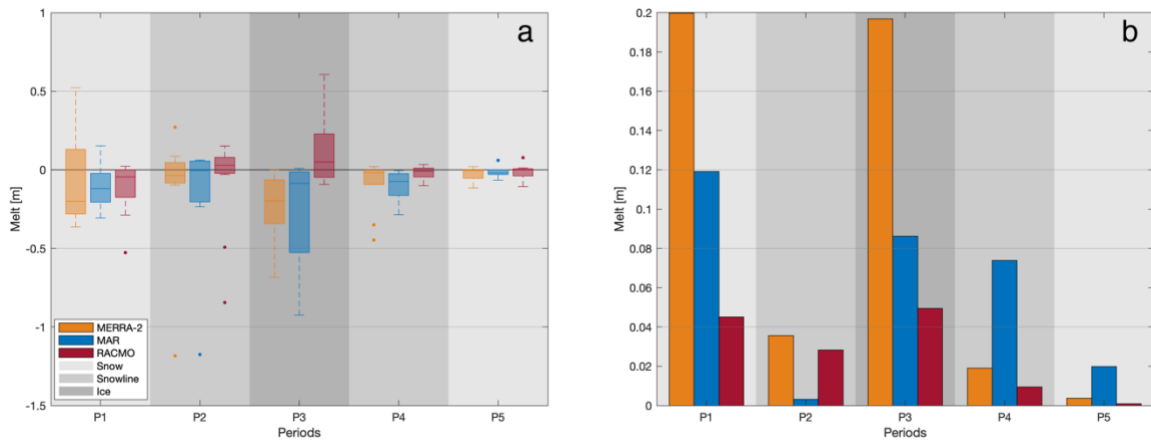
In the ablation zone, 1) the geometry of ice sheet boundaries, 2) a point's proximity to the ice sheet margin, and 3) latitude have a stronger influence on the observed albedo of glacier ice than elevation. For example, NUK-L (530 m) has an average summer albedo of 0.33 (Fig. 14a), while other "lower" stations, like THU-L (570 m), KPC-L (370 m), and UPE-L (220 m) have average summer albedos of 0.48, 0.48, and 0.52, respectively (Figs. 15-17a). Aside from the latter three stations being higher in latitude, NUK-L is also positioned on a marine-terminating glacier that extends from the ice sheet and is surrounded by a fjord. The following is also the case for SCO-L (460 m) and SCO-U (970 m), which are both positioned on a marine-terminating glacier and have average summer albedos of 0.37 and 0.43, respectively (Fig. 18). We stipulate that having bare-rock sides of a fjord surround an AWS that are finer than the grid cell scale is what causes the lowering in the surface albedo at the margins of the ice sheet with similar geometries. Lastly, the influence of latitude on observed glacier-ice albedo can be outlined by the juxtaposition of QAS-L (280 m) and UPE-L (220 m), in which the former is 18.9 degrees south of the latter (Table 2). Although both AWS are located on wide, land-terminating sides of the

26

GrIS (as opposed to a marine-terminating glacier in a relatively narrow fjord) and have similar elevations, the average summer albedo of UPE-L is 0.52, while it is 0.30 for QAS-L (Fig. 19a).
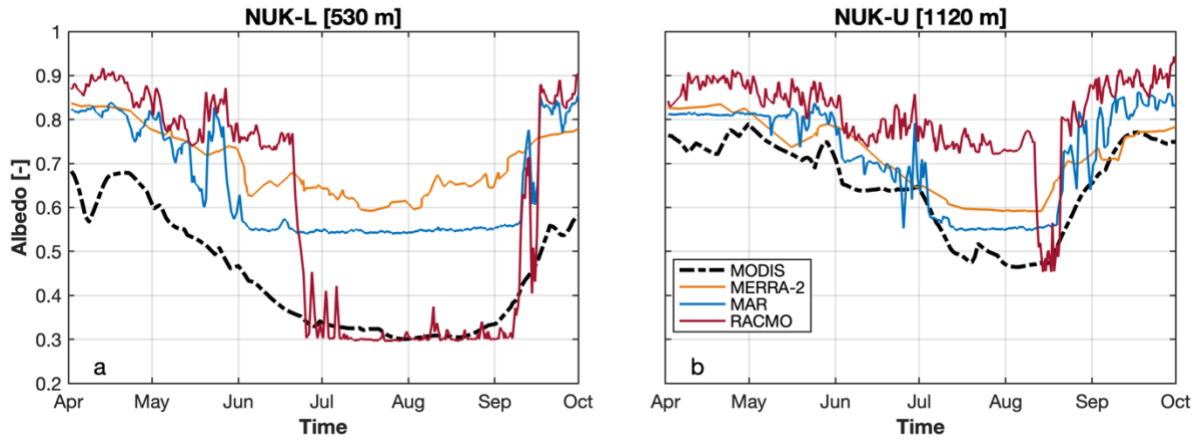
Figure 14. Average albedos of all models in the study at a) NUK-L, b) NUK-U.
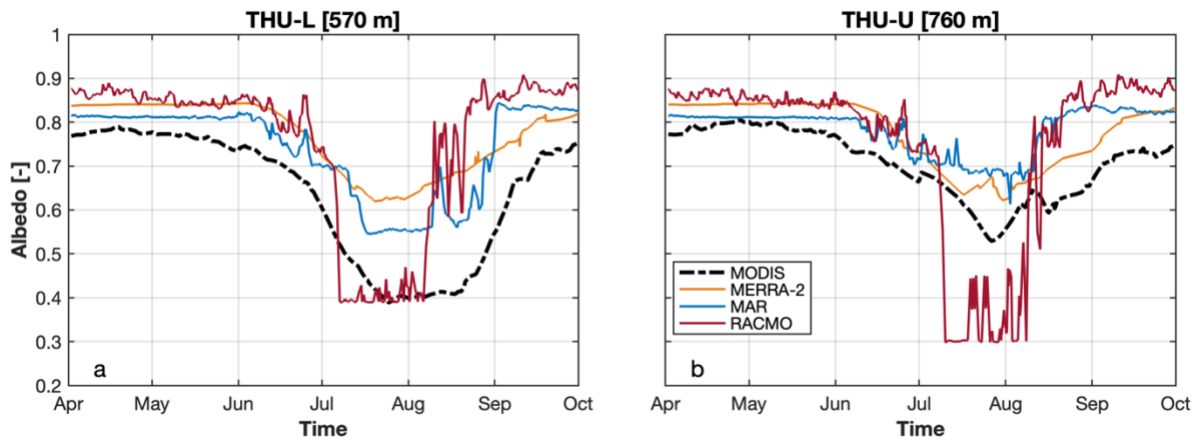
Figure 15. Average albedos of all models in the study at a) THU-L, b) THU-U.
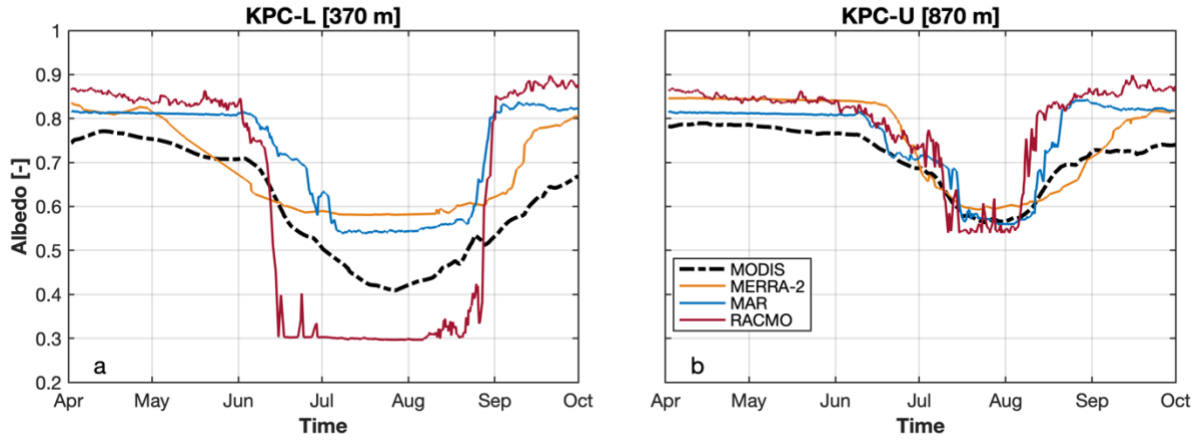
Figure 16. Average albedos of all models in the study at a) KPC-L, b) KPC-U.
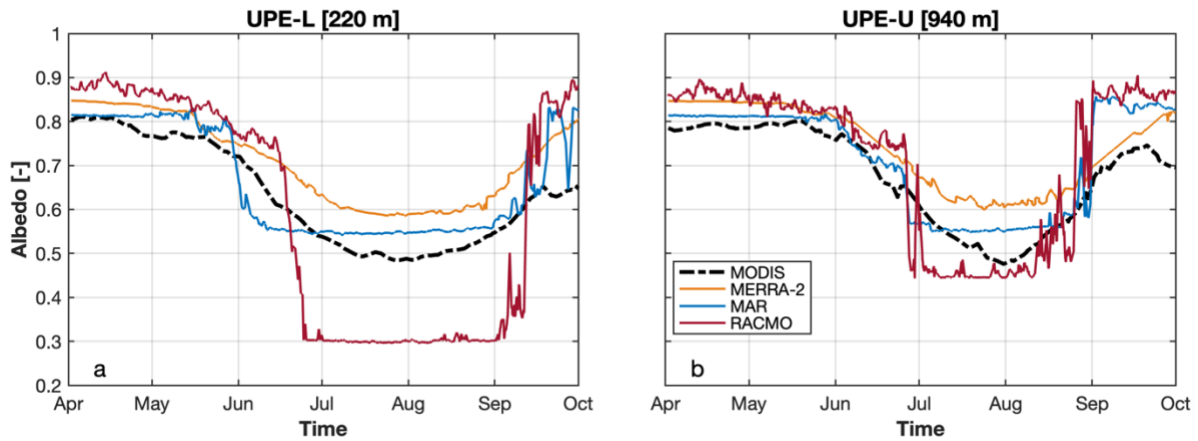
Figure 17. Average albedos of all models in the study at a) UPE-L, b) UPE-U.
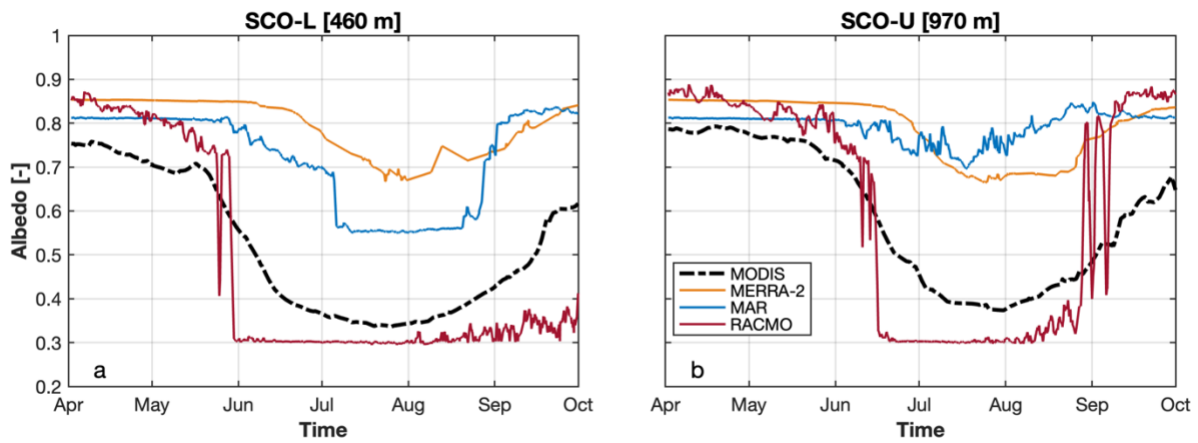
Figure 18. Average albedos of all models in the study at a) SCO-L, b) SCO-U.
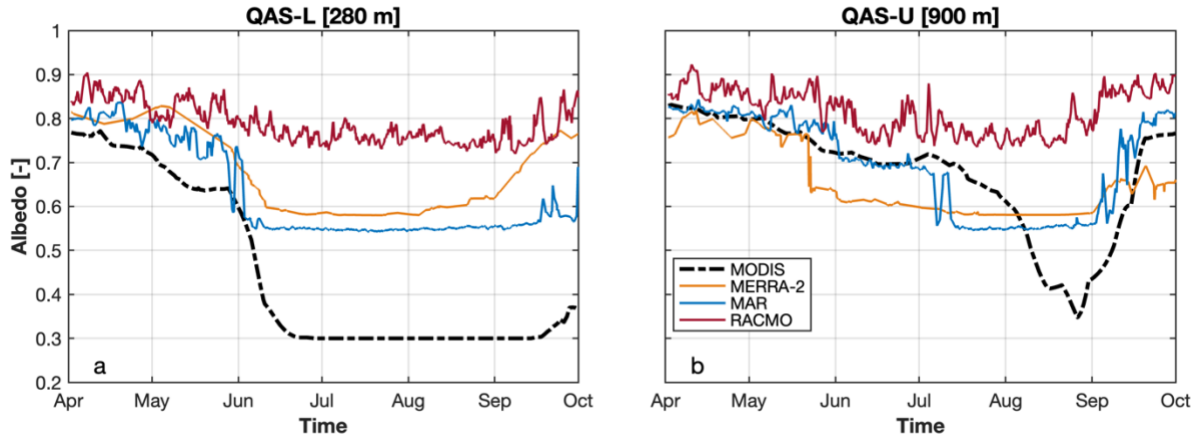
Figure 19. Average albedos of all models in the study at a) QAS-L, b) QAS-U.

RACMO generally always underestimates glacier ice albedo; however, at the southernmost sites (QAS-L & QAS-U), RACMO predicted the highest average albedo than all other models and observations (Fig. 19). While the average observed summer albedo at QAS-L and QAS-U is 0.30 and 0.68, respectively, RACMO simulates the summer albedo to be 0.76 and 0.77, respectively, at these sites. Overestimation of summer albedo in such a manner can serve as a counterbalance to the instances when RACMO underestimates it, resulting in simulations that are closer to observations. In other words, RACMO's albedo parameterization can correct itself, but via strong over-/underestimations at different locations and not necessarily via accurate albedo representation.

4. DISCUSSION

We use an SEB model to investigate the effect of albedo parameterizations on meltwater production across the GrIS. We isolate the effect of albedo using a sensitivity analysis, in which a flexible point-based SEB model is forced with the same hourly physical parameters (derived from the fifteen AWSs), but albedo is replaced to match modeled albedo from other sources. Our analysis enables us to attribute differences in meltwater production solely to discrepancies in modeled albedo. At the K-transect, we notice general trends of MERRA-2 and MAR underestimating (-20.3% and -28.6%, respectively) and RACMO overestimating (+11.6) summer melt (i.e., melt produced solely during exposed glacier ice). The majority of these biases are due to inaccurately modeled albedo at the lower elevation sites. For example, the mean RMSE in melt, for all models relative to observed, is ±0.94 m at KAN-L, ±0.66 m at KAN-M, and ±0.31 m at KAN-U (Fig. 7). We find similar under- and overestimation of melt due to albedo parameterizations across six pairs of AWS located in other regions of the ice sheet: MERRA-2 and MAR underestimate melt by -13.5% and -5.9%, respectively, while RACMO overestimates it by +3.4% relative to observations. The RMSE in melt is also higher at lower elevation sites than the upper sites. For example, RMSE in melt is ±1.11 m for the "L" sites with a mean elevation of 405 m and ±0.68 m for the "U" sites with a mean elevation of 927 m (Table 2, Figs. 14-19).

4.1. Glacier ice albedo

By partitioning our analysis into five different periods of the melt season, we find that most of the higher RMSE in melt at the lower sites can be attributed to differences between observed and modeled glacier ice albedo. The fixed glacier ice albedo in MERRA-2 (0.60) has a general tendency to overestimate glacier ice albedo relative to satellite observations (+0.11 [+24.4%] at K-transect, +0.13 [+27.5%] across AWS). Similarly, MAR overestimates glacier ice albedo (K-transect: +0.10 [+23.6%], all AWS: +0.11 [+25.8%]). This finding is consistent with other studies that compared albedo from various versions of MAR (v2.0, v3.2, and v3.12; the latter version was used in this study) to albedo data from PROMICE/GC-Net AWSs and MODIS products (MOD10A1, MOD09GA, and MCD43A3; the latter was used in this study), and found an overall positive bias in the ablation zone relative to observations (Alexander et al., 2014;

Antwerpen et al., 2022). In contrast, RACMO consistently underestimates glacier ice albedo (K-transect: -0.07 [-14.7%]; all AWS: -0.07 [-15.7%]).

Glacier ice albedo is challenging to simulate accurately due to the number of processes that can influence it. High-resolution drone imagery across southwestern Greenland indicates that glacier ice albedo is modified by crevasses, ponding of meltwater, light-absorbing impurities, and cryoconite (Ryan, Hubbard, Box, et al., 2017). Due to the complexity of these processes, even the latest generation of RCMs do not yet simulate glacier ice albedo in a physically-based way. Instead, each model uses a different method for parameterizing the albedo of glacier ice. For MERRA-2, a value of 0.60 is assigned to both represent glacier ice across the entire ice sheet (Cullather et al., 2014). However, observed glacier ice albedo averages 0.42 in the summer at our "L" sites and can be as low as 0.30 at QAS-L. The fixed glacier ice albedo value used by MERRA-2 is therefore almost always too high, leading to consistent underestimation of summer melt. The use of a more widely accepted glacier ice albedo value (e.g. 0.55), would therefore provide an immediate improvement in MERRA-2 meltwater predictions (Fettweis et al., 2017; Ryan et al., 2019; van Angelen et al., 2012). The albedo of glacier in MAR is also relatively fixed. Despite claiming to parametrically account for dirty ice that can go as low as 0.50, we find that glacier ice albedo averages 0.54 at our AWS. Therefore, like MERRA-2, MAR overestimates glacier ice albedo and underestimates summer meltwater production (Fig. 6a). RACMO takes a different approach by prescribing glacier ice albedo as the 5th percentile of albedo from MCD43A3 averaged between 2000 and 2015. The advantage of this approach is that it captures the spatial variability in glacier ice albedo. For example, observed glacier albedo averages 0.52 at UPE-L but 0.30 at QAS-L. However, by choosing the 5th percentile, RACMO consistently underestimates glacier ice albedo during our study period resulting in overestimated melt production (Figs. 9a & 12a). The mean albedo from the MCD43A3 product might therefore be more appropriate for prescribing glacier ice albedo and reducing this bias.

4.2. Snow albedo

In contrast to glacier ice albedo, all models generally simulate snow albedo accurately relative to observations. Interestingly, the atmospheric reanalysis product (MERRA-2) simulates albedo most accurately compared to observations at both the K-transect (Fig. 8a) and across all

AWS (Fig. 11b). MAR slightly underestimates snow albedo and RACMO tends to slightly overestimate snow albedo. One possible reason for a better representation of snow albedo versus that of glacier ice is the models' varying degrees of attention to detail and applications of constraints to snow and albedo parameterizations. Within its framework, each model includes a snow module that accounts for many snowpack-related processes, such as meltwater percolation, changes in impurity concentrations, and snow grain size evolution. By applying physically based modules for representing the snowpack, models produce snow albedo estimates that match closely with observations.

4.3. Timing of glacier ice exposure

All models simulate the timing of glacier ice exposure relatively well. Generally, RACMO exposes glacier ice sooner than observations (by 5.7 days across all AWS), while MERRA-2 and MAR expose it 6.7 and 4.0 days later, respectively. However, when it comes to representing the total duration of glacier ice exposure, RACMO agrees on the most days with observations (Fig. 13), resulting in the longest duration of glacier ice exposure (51.6 days). We speculate that this is the reason behind RACMO ultimately resulting in the highest meltwater production estimates relative to other models. In order to capture the exposure of glacier ice representatively, models must have well-calibrated melt rates and accurate antecedent snowfall. Thus, all models perform particularly well in timing the exposure of glacier ice (i.e., doing within several days as opposed to several weeks).

4.4. Compensating effects

We find some cases where the under-/overestimation of snow albedo combined with the over-/underestimation of glacier ice albedo has a counteractive effect that reduces overall uncertainty in summer meltwater production. For example, RACMO, as a result of simulating darker glacier-ice albedo relative to observations (-0.07 [-15.7%]), produces more meltwater (+0.05 m [+4.8%]) during the ablation season as a consequence of the melt-albedo feedback; however, because RACMO also simulates a brighter snow albedo (+0.052 [+6.2%]), there will be less melt produced (-0.045 m [-30.3%]) during those periods, resulting in a smaller cumulative meltwater estimate at the end of the year. MERRA-2 and MAR exhibit compensating effects in the representation of albedo that are opposite to those of RACMO. In other words,

32

MERRA-2 and MAR tend to underestimate snow albedo and overestimate glacier ice albedo (Fig. 11a). The presence of counteracting effects is concerning because it can cause the uncertainty to appear smaller than it truly is. This can have direct implications on future simulations of these processes; for example, if there will be an increase in glacier ice exposure, then there can be unanticipated biases in both melt and its uncertainty. It is the presence of these compensating errors like these that could be responsible for a finding of GrSMBMIP, which highlighted that utilizing an ensemble mean of different models yields the optimal SMB estimates relative to observations (Fettweis et al., 2020).

4.5.   Reflection and limitations

Our analysis extends previous research that had investigated the accuracy of modeled albedo in RCM and atmospheric reanalysis. Alexander et al. (2014) compared different MODIS products (including MCD43A3 that is used in this study) with several versions of the MAR RCM for 2000-2013 to assess the spatio-temporal variability of albedo on the GrIS. Building on that work, Antwerpen et al. (2022) quantified the effects of MAR's glacier ice albedo on meltwater estimates and compared them to MODIS albedo across Greenland below 70ºN. In our study, we perform a more in-depth investigation of how albedo errors impact melt holistically and across different surface types. By employing the basic principles of a sensitivity analysis, we are able to isolate the effects of albedo on meltwater estimates, which can be difficult to achieve in intercomparison studies.

Having said that, there are some limitations in our study that should be discussed. One is that the simulated albedo we use to force IceModel could have been produced under slightly different forcings. For example, differences in snow albedo between the models could be explained by differences in model air temperatures, as opposed to their albedo parametrizations. However, it is unlikely that this had a major impact on our findings since both RACMO and MAR are forced by ERA-5, meaning that they likely have very similar boundary conditions. Another limitation is the use of AWS forcing data. Although the instruments are designed to record hourly data of each meteorological variable (Table 1), there are often data gaps. Large gaps in the AWS albedo data, for example, was the main reason for replacing that data with satellite observations of albedo. Other data gaps are caused by instrument failure, toppling of the AWS, and/or other issues that arise as a result of being exposed to extreme climatic conditions

33

on the ice sheet (Fausto et al., 2021). To account for this, we only used AWS when a full year of data was available (Fig. 3).

4.6. Outlook

The goal of this study was to highlight the importance of albedo parameterizations on meltwater production in the latest generation of RCMs and atmospheric reanalysis. All models used in this study are well-known and widely used by the glaciological community, especially for studies of SMB across the Greenland and Antarctic ice sheets. Given that glacier ice accounts for a substantial portion of meltwater production, it is particularly important that the representation of glacier ice albedo is accurate. We acknowledge, however, that modeling glacier ice albedo in a physically-based way, like snow albedo, is easier said than done. We therefore hope that our results, which highlight specific shortcomings, can provide modelers with more context when making decisions about improvements of RCMs. Doing so will further reduce the uncertainty in model outputs and their representation of the GrIS SMB, especially that of glacier ice in the ablation zone, more realistic.

5. CONCLUSIONS

In this study, we investigated how different parameterizations of surface albedo impact melt on the Greenland Ice Sheet of two regional climate models (RACMO2.3p2, MARv3.12.1), a global atmospheric reanalysis product (MERRA-2, M2T3NXGLCv5.12.4), and satellite observations (MODIS, MCD43A3v6.1). This allowed us to highlight any discrepancies that the models have with observations regarding the representation of surface albedo, particularly on the edges of the ice sheet, and identify any possible explanations for the differences. Our study area was constrained to point locations of fifteen automated weather stations located across the ice sheet which have reliable meteorological data within the ablation zone or its vicinity. We performed a sensitivity analysis with a surface energy balance model, IceModel, to produce meltwater production estimates with albedo from the models and satellite observations. We then averaged (median) across all stations and for the years 2009-2022 to investigate the extent to which biases of each model's albedo cause differences in melt, relative to observations. Although averaging across all weather stations covers some degree of unique variability that occurs at each site, this technique allows for a more holistic understanding of model performance in the ablation zone of the Greenland Ice Sheet. It is important to reiterate that the meltwater production estimates shown in this study are *not* forecasts by the named models, but rather meltwater predictions made by IceModel driven with simulated *albedo* of the models.

Our results demonstrate that, relative to satellite observations, MAR and MERRA-2 albedo parameterizations lead to an underestimation of cumulative meltwater (-0.60 m [-36.3%] and -0.45 m [-27.1%], respectively), while RACMO slightly overestimates end of the year melt (+0.091 m [5.5%]). The under-/overestimation of melt is a function of snow and glacier ice albedo values, as well as the initial and total exposure of glacier ice. Both MAR and MERRA-2 tend to overestimate glacier ice albedo (by +0.11 and +0.13, respectively), expose glacier ice later (by 4 and 6.7 days, respectively) and cover it with snow earlier (by 26 and 12 days, respectively), than observations. RACMO tends to underestimate glacier ice albedo (by -0.07) and expose glacier ice earlier than observations (by 5.7 days), but, like MAR and MERRA-2, also covers glacier ice earlier (by 2.5 days). We identify compensating effects, that are particularly noteworthy for RACMO which underestimates glacier ice albedo but simulates snow albedo that is brighter than observations. This results in less melt produced during snow periods,

35

which counteracts the increased meltwater production during summer (i.e., when glacier ice is exposed).

We speculate that the reason for RACMO's glacier ice albedo matching closest with observations is a result of RACMO utilizing satellite observations (namely, a MODIS product). Thus, one way in which developers of MAR and MERRA-2 can improve their glacier-albedo scheme is by using satellite observations to correct the glacier ice albedo produced by their models. Performing this, we believe, will significantly improve the model's representation of total time glacier ice is exposed. Additionally, the albedo schemes of each model can be improved by adjusting the constraints that each apply in their dataset. For MERRA-2 this would be to allow for lower values of glacier ice. For MAR, that claims to have an albedo scheme that allows the albedo to decrease to 0.5 for dirty ice, one suggestion is to match more closely with observations. For RACMO, the lowest 5% of glacier ice albedo results in overestimated meltwater production when glacier ice is exposed.

REFERENCES

Alexander, P. M., Tedesco, M., Fettweis, X., van de Wal, R. S. W., Smeets, C. J. P. P., & van den Broeke, M. R. (2014). Assessing spatio-temporal variability and trends in modelled and measured Greenland Ice Sheet albedo (2000–2013). *The Cryosphere*, *8*(6), 2293–2312. https://doi.org/10.5194/tc-8-2293-2014

Antwerpen, R. M., Tedesco, M., Fettweis, X., Alexander, P., & van de Berg, W. J. (2022). Assessing bare-ice albedo simulated by MAR over the Greenland ice sheet (2000–2021) and implications for meltwater production estimates. *The Cryosphere*, *16*(10), 4185–4199. https://doi.org/10.5194/tc-16-4185-2022

Box, J. E., Fettweis, X., Stroeve, J. C., Tedesco, M., Hall, D. K., & Steffen, K. (2012). Greenland ice sheet albedo feedback: Thermodynamics and atmospheric drivers. *The Cryosphere*, *6*(4), 821–839. https://doi.org/10.5194/tc-6-821-2012

Braithwaite, R. J., & Olesen, O. B. (1990). A Simple Energy-Balance Model to Calculate Ice Ablation at the Margin of the Greenland Ice Sheet. *Journal of Glaciology*, *36*(123), 222–228. https://doi.org/10.3189/S0022143000009473

Brock, B. W., Willis, I. C., Sharp, M. J., & Arnold, N. S. (2000). Modelling seasonal and spatial variations in the surface energy balance of Haut Glacier d'Arolla, Switzerland. *Annals of Glaciology*, *31*, 53–62. https://doi.org/10.3189/172756400781820183

Brun, E., David, P., Sudul, M., & Brunot, G. (1992). A numerical model to simulate snow-cover stratigraphy for operational avalanche forecasting. *Journal of Glaciology*, *38*(128), 13–22. https://doi.org/10.3189/S0022143000009552

Cooper, M. G., Smith, L. C., Rennermalm, A. K., Tedesco, M., Muthyala, R., Leidman, S. Z., Moustafa, S. E., & Fayne, J. V. (2021). Spectral attenuation coefficients from

measurements of light transmission in bare ice on the Greenland Ice Sheet. *The Cryosphere*, *15*(4), 1931–1953. https://doi.org/10.5194/tc-15-1931-2021

Cooper, M., Smith, L., Rennermalm, Å., Yang, K., Liston, G., Ryan, J., As, D. V., Pitcher, L., Miège, C., Cooley, S., & Overstreet, B. (2021). *Greenland Ice Sheet runoff reduced by meltwater refreezing in bare ice* [Preprint]. In Review. https://doi.org/10.21203/rs.3.rs-842710/v1

Cullather, R. I., Nowicki, S. M. J., Zhao, B., & Suarez, M. J. (2014). Evaluation of the Surface Representation of the Greenland Ice Sheet in a General Circulation Model. *Journal of Climate*, *27*(13), 4835–4856. https://doi.org/10.1175/JCLI-D-13-00635.1

Enderlin, E. M., Howat, I. M., Jeong, S., Noh, M.-J., van Angelen, J. H., & van den Broeke, M. R. (2014). An improved mass budget for the Greenland ice sheet. *Geophysical Research Letters*, *41*(3), 866–872. https://doi.org/10.1002/2013GL059010

Ettema, J., van den Broeke, M. R., van Meijgaard, E., van de Berg, W. J., Box, J. E., & Steffen, K. (2010). Climate of the Greenland ice sheet using a high-resolution climate model – Part 1: Evaluation. *The Cryosphere*, *4*(4), 511–527. https://doi.org/10.5194/tc-4-511-2010

Fausto, R. S., van As, D., Mankoff, K. D., Vandecrux, B., Citterio, M., Ahlstrøm, A. P., Andersen, S. B., Colgan, W., Karlsson, N. B., Kjeldsen, K. K., Korsgaard, N. J., Larsen, S. H., Nielsen, S., Pedersen, A. Ø., Shields, C. L., Solgaard, A. M., & Box, J. E. (2021). Programme for Monitoring of the Greenland Ice Sheet (PROMICE) automatic weather station data. *Earth System Science Data*, *13*(8), 3819–3845. https://doi.org/10.5194/essd-13-3819-2021

Fettweis, X. (2007). Reconstruction of the 1979–2006 Greenland ice sheet surface mass

    balance using the regional climate model MAR. *The Cryosphere*, *1*(1), 21–40.

    https://doi.org/10.5194/tc-1-21-2007

Fettweis, X., Box, J. E., Agosta, C., Amory, C., Kittel, C., Lang, C., van As, D., Machguth, H.,

    & Gallée, H. (2017). Reconstructions of the 1900–2015 Greenland ice sheet surface mass

    balance using the regional climate MAR model. *The Cryosphere*, *11*(2), 1015–1033.

    https://doi.org/10.5194/tc-11-1015-2017

Fettweis, X., Franco, B., Tedesco, M., van Angelen, J. H., Lenaerts, J. T. M., van den Broeke, M.

    R., & Gallée, H. (2013). Estimating the Greenland ice sheet surface mass balance

    contribution to future sea level rise using the regional atmospheric climate model MAR.

    The Cryosphere, *7*(2), 469–489. https://doi.org/10.5194/tc-7-469-2013

Fettweis, X., Hofer, S., Krebs-Kanzow, U., Amory, C., Aoki, T., Berends, C. J., Born, A., Box, J.

    E., Delhasse, A., Fujita, K., Gierz, P., Goelzer, H., Hanna, E., Hashimoto, A.,

    Huybrechts, P., Kapsch, M.-L., King, M. D., Kittel, C., Lang, C., … Zolles, T. (2020).

    GrSMBMIP: Intercomparison of the modelled 1980–2012 surface mass balance over the

    Greenland Ice Sheet. *The Cryosphere*, *14*(11), 3935–3958. https://doi.org/10.5194/tc-14-

    3935-2020

Fettweis, X., Tedesco, M., van den Broeke, M., & Ettema, J. (2011). Melting trends over the

    Greenland ice sheet (1958–2009) from spaceborne microwave data and regional climate

    models. *The Cryosphere*, *5*(2), 359–375. https://doi.org/10.5194/tc-5-359-2011

Global Modeling and Assimilation Office (GMAO). (2015). *MERRA-2 tavg3_2d_glc_Nx: 2d,3-*

    Hourly,Time-Averaged,Single-Level,Assimilation,Land Ice Surface Diagnostics V5.12.4,

    Greenbelt, MD, USA, Goddard Earth Sciences Data and Information Services Center

(GES DISC).

https://disc.gsfc.nasa.gov/datasets/M2T3NXGLC_5.12.4/summary?keywords=M2T3NX

GLC_5.12.4

Greuell, W., & Konzelmann, T. (1994). Numerical modelling of the energy balance and the

englacial temperature of the Greenland Ice Sheet. Calculations for the ETH-Camp

location (West Greenland, 1155 m a.s.l.). *Global and Planetary Change*, *9*(1), 91–114.

https://doi.org/10.1016/0921-8181(94)90010-8

Hersbach, H., Bell, B., Berrisford, P., Hirahara, S., Horányi, A., Muñoz-Sabater, J., Nicolas, J.,

Peubey, C., Radu, R., Schepers, D., Simmons, A., Soci, C., Abdalla, S., Abellan, X.,

Balsamo, G., Bechtold, P., Biavati, G., Bidlot, J., Bonavita, M., … Thépaut, J.-N. (2020).

The ERA5 global reanalysis. *Quarterly Journal of the Royal Meteorological Society*,

146(730), 1999–2049. https://doi.org/10.1002/qj.3803

Knap, W., & Oerlemans, J. (1996). The surface albedo of the Greenland ice sheet: Satellite-

derived and in situ measurements in the Søndre Strømfjord area during the 1991 melt

season. *Journal of Glaciology*, *42*. https://doi.org/10.1017/S0022143000004214

Konzelmann, T., & Ohmura, A. (1995). Radiative fluxes and their impact on the energy balance

of the Greenland ice sheet. *Journal of Glaciology*, *41*(139), 490–502.

https://doi.org/10.3189/S0022143000034833

Lefebre, F., Gallée, H., van Ypersele, J.-P., & Greuell, W. (2003). Modeling of snow and ice

melt at ETH Camp (West Greenland): A study of surface albedo. *Journal of Geophysical

Research: Atmospheres*, *108*(D8). https://doi.org/10.1029/2001JD001160

Liston, G. E., Winther, J.-G., Bruland, O., Elvehøy, H., & Sand, K. (1999). Below-surface ice melt on the coastal Antarctic ice sheet. *Journal of Glaciology*, *45*(150), 273–285. https://doi.org/10.3189/S0022143000001775

Molod, A., Takacs, L., Suarez, M., & Bacmeister, J. (2015). Development of the GEOS-5 atmospheric general circulation model: Evolution from MERRA to MERRA2. *Geoscientific Model Development*, *8*, 1339–1356. https://doi.org/10.5194/gmd-8-1339-2015

Noël, B., van de Berg, W. J., Lhermitte, S., & van den Broeke, M. R. (2019). Rapid ablation zone expansion amplifies north Greenland mass loss. *Science Advances*, *5*(9), eaaw0123. https://doi.org/10.1126/sciadv.aaw0123

Otosaka, I. N., Shepherd, A., Ivins, E. R., Schlegel, N.-J., Amory, C., van den Broeke, M. R., Horwath, M., Joughin, I., King, M. D., Krinner, G., Nowicki, S., Payne, A. J., Rignot, E., Scambos, T., Simon, K. M., Smith, B. E., Sørensen, L. S., Velicogna, I., Whitehouse, P. L., … Wouters, B. (2023). Mass balance of the Greenland and Antarctic ice sheets from 1992 to 2020. *Earth System Science Data*, *15*(4), 1597–1616. https://doi.org/10.5194/essd-15-1597-2023

Pitcher, L. H., & Smith, L. C. (2019). Supraglacial Streams and Rivers. *Annual Review of Earth and Planetary Sciences*, *47*(1), 421–452. https://doi.org/10.1146/annurev-earth-053018-060212

Rae, J. G. L., Aðalgeirsdóttir, G., Edwards, T. L., Fettweis, X., Gregory, J. M., Hewitt, H. T., Lowe, J. A., Lucas-Picher, P., Mottram, R. H., Payne, A. J., Ridley, J. K., Shannon, S. R., van de Berg, W. J., van de Wal, R. S. W., & van den Broeke, M. R. (2012). Greenland ice sheet surface mass balance: Evaluating simulations and making projections with regional

climate models. *The Cryosphere*, *6*(6), 1275–1294. https://doi.org/10.5194/tc-6-1275-2012

Rennermalm, A. K., Smith, L. C., Chu, V. W., Box, J. E., Forster, R. R., Van den Broeke, M. R., Van As, D., & Moustafa, S. E. (2013). Evidence of meltwater retention within the Greenland ice sheet. *The Cryosphere*, *7*(5), 1433–1445. https://doi.org/10.5194/tc-7-1433-2013

Ryan, J. C., Hubbard, A., Box, J. E., Brough, S., Cameron, K., Cook, J. M., Cooper, M., Doyle, S. H., Edwards, A., Holt, T., Irvine-Fynn, T., Jones, C., Pitcher, L. H., Rennermalm, A. K., Smith, L. C., Stibal, M., & Snooke, N. (2017). Derivation of High Spatial Resolution Albedo from UAV Digital Imagery: Application over the Greenland Ice Sheet. *Frontiers in Earth Science*, *5*. https://doi.org/10.3389/feart.2017.00040

Ryan, J. C., Hubbard, A., Irvine-Fynn, T. D., Doyle, S. H., Cook, J. M., Stibal, M., & Box, J. E. (2017). How robust are in situ observations for validating satellite-derived albedo over the dark zone of the Greenland Ice Sheet? *Geophysical Research Letters*, *44*(12), 6218–6225. https://doi.org/10.1002/2017GL073661

Ryan, J. C., Smith, L. C., van As, D., Cooley, S. W., Cooper, M. G., Pitcher, L. H., & Hubbard, A. (2019). Greenland Ice Sheet surface melt amplified by snowline migration and bare ice exposure. *Science Advances*, *5*(3), eaav3738. https://doi.org/10.1126/sciadv.aav3738

Schaaf, C. B., Gao, F., Strahler, A. H., Lucht, W., Li, X., Tsang, T., Strugnell, N. C., Zhang, X., Jin, Y., Muller, J.-P., Lewis, P., Barnsley, M., Hobson, P., Disney, M., Roberts, G., Dunderdale, M., Doll, C., d'Entremont, R. P., Hu, B., … Roy, D. (2002). First operational BRDF, albedo nadir reflectance products from MODIS. *Remote Sensing of Environment*, *83*(1–2), 135–148. https://doi.org/10.1016/S0034-4257(02)00091-3

Schaaf, C., & Wang, Z. (2021). *MODIS/Terra+Aqua BRDF/Albedo Daily L3 Global—500m V061* [dataset]. https://doi.org/10.5067/MODIS/MCD43A3.061

Shepherd, A., Ivins, E., Rignot, E., Smith, B., van den Broeke, M., Velicogna, I., Whitehouse, P., Briggs, K., Joughin, I., Krinner, G., Nowicki, S., Payne, T., Scambos, T., Schlegel, N., A, G., Agosta, C., Ahlstrøm, A., Babonis, G., Barletta, V. R., … The IMBIE Team. (2020). Mass balance of the Greenland Ice Sheet from 1992 to 2018. *Nature*, *579*(7798), 233–239. https://doi.org/10.1038/s41586-019-1855-2

Smith, L. C., Chu, V. W., Yang, K., Gleason, C. J., Pitcher, L. H., Rennermalm, A. K., Legleiter, C. J., Behar, A. E., Overstreet, B. T., Moustafa, S. E., Tedesco, M., Forster, R. R., LeWinter, A. L., Finnegan, D. C., Sheng, Y., & Balog, J. (2015). Efficient meltwater drainage through supraglacial streams and rivers on the southwest Greenland ice sheet. *Proceedings of the National Academy of Sciences*, *112*(4), 1001–1006. https://doi.org/10.1073/pnas.1413024112

Smith, L. C., Yang, K., Pitcher, L. H., Overstreet, B. T., Chu, V. W., Rennermalm, Å. K., Ryan, J. C., Cooper, M. G., Gleason, C. J., Tedesco, M., Jeyaratnam, J., van As, D., van den Broeke, M. R., van de Berg, W. J., Noël, B., Langen, P. L., Cullather, R. I., Zhao, B., Willis, M. J., … Behar, A. E. (2017). Direct measurements of meltwater runoff on the Greenland ice sheet surface. *Proceedings of the National Academy of Sciences*, *114*(50), E10622–E10631. https://doi.org/10.1073/pnas.1707743114

Steger, C. R., Reijmer, C. H., & van den Broeke, M. R. (2017). The modelled liquid water balance of the Greenland Ice Sheet. *The Cryosphere*, *11*(6), 2507–2526. https://doi.org/10.5194/tc-11-2507-2017

Stieglitz, M., Ducharne, A., Koster, R., & Suarez, M. (2001). The Impact of Detailed Snow

    Physics on the Simulation of Snow Cover and Subsurface Thermodynamics at

    Continental Scales. *Journal of Hydrometeorology*, *2*(3), 228–242.

    https://doi.org/10.1175/1525-7541(2001)002<0228:TIODSP>2.0.CO;2

Stroeve, J., Box, J. E., Gao, F., Liang, S., Nolin, A., & Schaaf, C. (2005). Accuracy assessment

    of the MODIS 16-day albedo product for snow: Comparisons with Greenland in situ

    measurements. *Remote Sensing of Environment*, *94*(1), 46–60.

    https://doi.org/10.1016/j.rse.2004.09.001

Tedesco, M., & Fettweis, X. (2020). Unprecedented atmospheric conditions (1948–2019) drive

    the 2019 exceptional melting season over the Greenland ice sheet. *The Cryosphere*,

    14(4), 1209–1223. https://doi.org/10.5194/tc-14-1209-2020

van Angelen, J. H., Lenaerts, J. T. M., Lhermitte, S., Fettweis, X., Kuipers Munneke, P., van den

    Broeke, M. R., van Meijgaard, E., & Smeets, C. J. P. P. (2012). Sensitivity of Greenland

    Ice Sheet surface mass balance to surface albedo parameterization: A study with a

    regional climate model. *The Cryosphere*, *6*(5), 1175–1186. https://doi.org/10.5194/tc-6-

    1175-2012

Van As, D., Fausto, R. S., Colgan, W. T., Box, J. E., & Promice Project Team, *. (2013).

    Darkening of the Greenland ice sheet due to the melt albedo feedback observed at

    PROMICE weather stations. *Geological Survey of Denmark and Greenland Bulletin*, *28*,

    69–72. https://doi.org/10.34194/geusb.v28.4728

van den Broeke, M., Bamber, J., Ettema, J., Rignot, E., Schrama, E., van de Berg, W. J., van

    Meijgaard, E., Velicogna, I., & Wouters, B. (2009). Partitioning Recent Greenland Mass

    Loss. *Science*, *326*(5955), 984–986. https://doi.org/10.1126/science.1178176

van den Broeke, M., Box, J., Fettweis, X., Hanna, E., Noël, B., Tedesco, M., van As, D., van de Berg, W. J., & van Kampenhout, L. (2017). Greenland Ice Sheet Surface Mass Loss: Recent Developments in Observation and Modeling. *Current Climate Change Reports*, *3*(4), 345–356. https://doi.org/10.1007/s40641-017-0084-8

van den Broeke, M. R., Enderlin, E. M., Howat, I. M., Kuipers Munneke, P., Noël, B. P. Y., van de Berg, W. J., van Meijgaard, E., & Wouters, B. (2016). On the recent contribution of the Greenland ice sheet to sea level change. *The Cryosphere*, *10*(5), 1933–1946. https://doi.org/10.5194/tc-10-1933-2016

van den Broeke, M. R., Smeets, C. J. P. P., & van de Wal, R. S. W. (2011). The seasonal cycle and interannual variability of surface energy balance and melt in the ablation zone of the west Greenland ice sheet. *The Cryosphere*, *5*(2), 377–390. https://doi.org/10.5194/tc-5-377-2011

Vernon, C. L., Bamber, J. L., Box, J. E., van den Broeke, M. R., Fettweis, X., Hanna, E., & Huybrechts, P. (2013). Surface mass balance model intercomparison for the Greenland ice sheet. *The Cryosphere*, *7*(2), 599–614. https://doi.org/10.5194/tc-7-599-2013

Wehrlé, A., Box, J. E., Niwano, M., Anesio, A. M., & Fausto, R. S. (2021). Greenland bare-ice albedo from PROMICE automatic weather station measurements and Sentinel-3 satellite observations. *GEUS Bulletin*, *47*. https://doi.org/10.34194/geusb.v47.5284

Yang, K., Smith, L. C., Karlstrom, L., Cooper, M. G., Tedesco, M., van As, D., Cheng, X., Chen, Z., & Li, M. (2018). A new surface meltwater routing model for use on the Greenland Ice Sheet surface. *The Cryosphere*, *12*(12), 3791–3811. https://doi.org/10.5194/tc-12-3791-2018